The Astrophysical Journal, 784:138 (6pp), 2014 April 1 doi:10.1088/0004-637X/784/2/138

AN EMPIRICAL DETERMINATION OF THE INTERGALACTIC BACKGROUND LIGHT USING NEAR-INFRARED DEEP GALAXY SURVEY DATA OUT TO 5 μm AND THE GAMMA-RAY OPACITY OF THE UNIVERSE

Sean T. Scully[1], Matthew A. Malkan[2], and Floyd W. Stecker[2,3]
[1] Department of Physics and Astronomy, James Madison University, Harrisonburg, VA 22807, USA
[2] Department of Physics and Astronomy, University of California, Los Angeles, CA 90095, USA; Floyd.W.Stecker@nasa.gov
[3] Astrophysics Science Division, NASA/Goddard Space Flight Center, 8800 Greenbelt Road, Greenbelt, MD 20771, USA
Received 2014 January 21; accepted 2014 February 24; published 2014 March 14

ABSTRACT

We extend our previous model-independent determination of the intergalactic background light, based purely on galaxy survey data, out to a wavelength of 5 μm. Our approach enables us to constrain the range of photon densities, based on the uncertainties from observationally determined luminosity densities and colors. We further determine a 68% confidence upper and lower limit on the opacity of the universe to γ-rays up to energies of $1.6/(1+z)$ TeV. A comparison of our lower limit redshift-dependent opacity curves to the opacity limits derived from the results of both ground-based air Cerenkov telescope and *Fermi*-LAT observations of PKS 1424+240 allows us to place a new upper limit on the redshift of this source, independent of IBL modeling.

Key words: BL Lacertae objects: individual (PKS 1424+240) – diffuse radiation – gamma rays: general

Online-only material: color figure

1. INTRODUCTION

Past work on estimating the spectral and redshift characteristics of the intergalactic photon density (IBL; with the $z = 0$ IBL usually referred to as the EBL) has depended on various assumptions as to the evolution of stellar populations and dust absorption in galaxies. There have also been attempts to probe the extragalactic background light (EBL) using studies of blazar γ-ray spectra (Ackermann et al. 2012; Abramowski et al. 2013), an approach originally suggested by Stecker et al. (1992).

We previously have pursued an independent, *fully empirical* approach to calculating the IBL using deep galaxy survey data (Stecker et al. 2012—hereafter SMS; see also Helgason & Kashlinsky 2012). In this paper, we extend the previous SMS results on the γ-ray opacity of the universe to TeV energies accessible to ground-based air Cerenkov telescopes, here including galaxy survey data extending beyond the photometric *I* band to the *M* band (i.e., 0.8 μm to $\sim$5 μm). We stress that the SMS approach, being completely observationally based, is *model independent*, relying only on published luminosity densities. Such an approach has a particular advantage over model-based methods, as it enables a determination of both the IBL *and its observational uncertainties* without making any assumptions about how the galaxy luminosity functions (LFs) evolve, as some approaches require (e.g. Malkan & Stecker 1998, 2001; Kneiske et al. 2002; Stecker et al. 2006; Franceschini et al. 2008; Finke et al. 2010; Kneiske & Dole 2010) or by using semi-analytic models that make assumptions concerning galaxy evolution, stellar population synthesis models, star formation rates, and dust attenuation (e.g., Gilmore et al. 2009; Somerville et al. 2012). Domínguez et al. (2011) used the redshift evolution of the *K*-band LFs of Cirasuolo et al. (2010), together with model templates based on *AEGIS* data to model the IBL. A recent detailed review of the problem has been given by Dwek & Krennrich (2013).

Direct integration of the galaxy survey data in the wavelength range from the far-ultraviolet (FUV) to $\sim$5 μm has now become possible. Observational data in this wavelength range, even out to redshifts $2 < z < 4$, have become sufficiently complete to eliminate the necessity of using model-based approaches. The high-redshift galaxies are sufficiently sampled to enable us to interpolate between observationally determined luminosity densities obtained for specific wavebands. We use observationally determined galaxy colors and their associated errors to fill in the gaps in wavelength bands where there are less data.

Here we apply the technique of SMS to determine the IBL to a wavelength of $\sim$5 μm, thus extending our previous range of γ-ray opacities of the universe to energies up to 1.6 TeV. This range is not only relevant for the sources with the highest redshifts observed by the *Fermi*-LAT Telescope, but also for results in the sub-TeV and TeV energy range made using ground-based air Cerenkov telescopes. Our technique to determine the expected γ-ray opacity of the universe is thus complementary to the technique of using γ-ray observations directly, because the intrinsic (unabsorbed) spectra of the γ-ray sources are uncertain.

To further show the utility of our approach, we apply our lower limit opacities to the results of both ground-based air Cerenkov telescope observations and *Fermi*-LAT observations of the BL Lac object PKS 1424+240, which allows us to place a *true upper limit* on the redshift of this source, independent of IBL models. Previous observations of the ultraviolet absorption from the intergalactic medium of this object place a *lower limit* on its redshift of $z \geqslant .6035$ (Furniss et al. 2013).

Our results give the γ-ray opacity as a function of energy and redshift to within an observationally determined 68% confidence band. Therefore, a direct comparison with γ-ray spectral data will allow an independent determination of the previously suggested effects on such spectra. These effects include secondary γ-ray production generated by (1) cosmic-ray interactions along the line of sight to the source (Essey et al. 2010; Essey & Kusenko 2012) and (2) line-of-sight photon–axion oscillations during propagation (e.g., De Angelis et al. 2007). Both of these processes can produce an apparent reduction of the pair-production opacity effect as derived from γ-ray spectra alone. Thus our results can be critical in analyzing the implications of present and future γ-ray spectral data.

2. DETERMINATION OF THE IBL FROM GALAXY PHOTON EMISSIVITIES

Galaxy LFs, $\Phi_\nu(L)$, can be determined by properly sampling galaxies in a survey for a given wavelength and accounting for biases. As in SMS, in this work, we chose to use only those references that give values for the integrated LF, i.e., the luminosity density (LD), $\rho_{L_\nu}(z)$. This is because there is generally a lack of knowledge about the covariance of the errors in the Schechter function parameters used to determine the dominant statistical errors in their analyses. Sufficient numbers of galaxies need to be observed up and down the LF for a reliable constraint on their total LD, i.e., the integral of the LF. It is not even guaranteed that a Schechter function will always provide the best analytic fit to the LF data. The co-moving radiation energy density, $u_\nu(z)$, is derived from the equivalent co-moving specific emissivity $\mathcal{E}_\nu(z) = \rho_{L_\nu}(z)$.

2.1. Luminosity Densities

In this work, we use the same set of galaxy survey data and resulting luminosity densities that covered rest-frame wavelengths from the FUV to the *I* band as in SMS; however, we now extend our calculations to the *J* and *K* bands. We have excluded the *H* band due to a paucity of observational data but we have checked that our approach is consistent with what data exists in this band. We further use the colors derived in the next subsection to extend the calculation into the *L* and *M* bands (out to 4.8 μm).

The co-moving radiation energy density $u_\nu(z)$ is the time integral of the co-moving specific emissivity $\mathcal{E}_\nu(z)$,

$$u_\nu(z) = \int_z^{z_{\max}} dz'\, \mathcal{E}_{\nu'}(z') \frac{dt}{dz}(z'), \quad (1)$$

where $\nu' = \nu(1+z')/(1+z)$ and $z_{\max}$ is the redshift corresponding to initial galaxy formation (Salamon & Stecker 1998), and

$$\frac{dt}{dz}(z) = [H_0(1+z)\sqrt{\Omega_\Lambda + \Omega_m(1+z)^3}]^{-1}, \quad (2)$$

with $\Omega_\Lambda = 0.72$ and $\Omega_m = 0.28$. We note that we have scaled all of the observational data for $\mathcal{E}_\nu(z)$ to a value of $h = 0.7$ for consistency.

2.2. Average Colors

The continuum emission from galaxies between 0.8 μm and 5 μm arises predominantly from stellar photospheres. At these near-infrared (NIR) wavelengths, the light is mostly emitted by red giant stars. Within a few million years of the first generation of star formation, massive stars will have left the main sequence to begin populating the red giant branch. At later times, red giant branch stars do not vary greatly from one stellar population to another. The resulting spectral energy distributions (SEDs) of galaxies are therefore much more similar to each other in the NIR range than they are at shorter wavelengths. The scatter in red and NIR SEDs of galaxies is especially small, since all of them contain old, red giant branch stellar populations, which dominate the stellar mass and the continuum emission around 1 μm.

Dai et al. (2009) determine galaxy LFs at 3.6, 4.5, 5.8, and 8.0 μm for a sample of 3800–5800 galaxies utilizing combined photometry from the *Spitzer*/IRAC Shallow Survey with redshifts from the active galactic nucleus and Galaxy Evolution Survey of the NOAO Deep Wide-Field Survey Boötes field. They obtained well defined complete LFs in the local redshift bin of $z \leqslant 0.2$. They then derived galaxy luminosity densities and generated a best-fit SED (their Figure 13). We take these data to be representative of low-redshift galaxies ($z \leqslant 0.5$).

Table 1
Average Colors

Waveband	Relative νL_ν	Std. Deviation	Min. Value	Max. Value
J (1.2 μm)	1[a]	–	–	–
H (1.6 μm)	1.19	0.08	1.09	1.37
K (2.2 μm)	0.97	0.12	0.83	1.23
L (3.5 μm)	0.70	0.15	0.43	0.99
M (4.8 μm)	0.50	0.16	0.3	0.84

Notes. The bias in the colors toward bluer averages occurs because there are not many galaxies in the very red categories, so the mean color stays on the blue side of (Max + Min)/2.
[a]All differences are relative to the *J* band.

To estimate the red and NIR SEDs of galaxies at higher redshifts, we have used the template SEDs derived by Kriek et al. (2010, 2011).[4] Those authors utilized extensive multiband photometry obtained for a sample of 3500 *K*-band selected galaxies, at redshifts between $z = 0.5$ and $z = 2.0$, close to a mass-limited sample of galaxies. For redshifts between $z = 0.5$ and $z = 1.0$, the galaxy stellar masses are uniformly distributed between the range of $10^{9.7}$ and $10^{11.3}$ $M_\odot$. At redshifts from 1 to 2, the mass range covered by these SEDs shrinks to $10^{10.3}$–$10^{11.3}$. Kriek et al. (2010) grouped their galaxy SEDs into 30 average templates spanning the full range from the bluest to the reddest galaxies. These typical L_* galaxies are the ones that produce most of the cosmic red and NIR emission. Therefore we take the unweighted average of the Kriek et al. (2010, 2011) SEDs to represent the full sample of galaxies. This should be reasonably accurate as there is only a 0.5 mag $Y - L$ color variation (from 1.05 to 3.5 μm) between the bluest and reddest galaxies. Therefore, over this full wavelength range, the *average* colors we have adopted must be quite close to the colors of any galaxy, at least at these redshifts. We express the average colors we have adopted as flux ratios normalized to *J* band in Table 1.

The peak in the galaxy SEDs that we used occurs around a rest wavelength of 1.6 μm. We note that there is a subtle trend for the red and NIR SEDs to become bluer at higher redshift. This is because the younger stellar populations were more important in the early universe. This effect produces a small shift of the SED peak to slightly shorter rest wavelengths at higher redshifts. This trend may continue to redshifts higher than two. However, because this effect is small, we assume that the SEDs of Kriek et al. (2010) apply to all higher redshifts. We assume that these average colors also apply to the less massive galaxies that Kriek et al. could not study. Fortunately, the total NIR emission of galaxies tends to be dominated by the more massive galaxies (e.g., Ly et al. 2011). Furthermore, galaxies of masses smaller by an order of magnitude are only slightly bluer.

2.3. Photon Density Calculations

As in SMS, we derive a luminosity confidence band in each of our additional wavebands by using a robust rational fitting function characterized by

$$\rho_{L_\nu} = \mathcal{E}_\nu(z) = \frac{ax + b}{cx^2 + dx + e}, \quad (3)$$

[4] See also http://astro.berkeley.edu/~mariska/comp/.

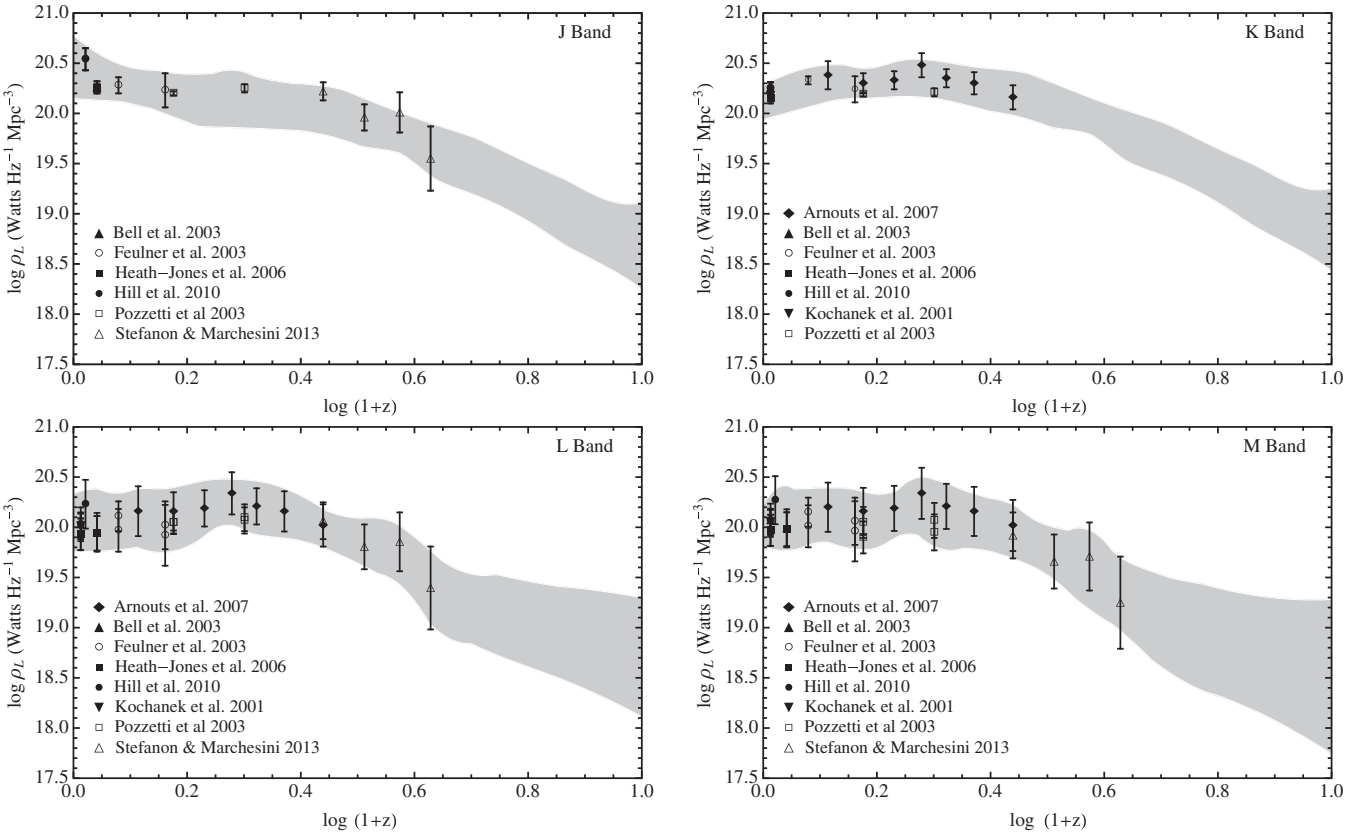

Figure 1. Specific emissivities for J, K, L, and M wavebands. In the L and M panels, the J- and K-band data have been shifted using the color relations given in the text in order to fully determine the specific emissivities in these wavebands. The gray shading represents the 68% confidence bands (see text).

where $x = \log(1 + z)$ and a, b, c, d, and e are free parameters. We compute the 68% confidence band from Monte Carlo simulations by finding 100,000 realizations of the data and then fitting the rational function given by Equation (3). As in SMS, we model symmetric error bars with a Gaussian distribution, while choosing a skew normal distribution to model asymmetric errors.

The K-band data do not extend beyond a redshift of $z \sim 2$, while the J-band data extend to $z \sim 3$. Thus, the fits determined using the above method can not be trusted beyond these limits. To handle this issue, we truncate our fits at a redshift of $z = 2$, and then color transform our previous I band from SMS to fit at the higher redshifts. This is a reasonable assumption owing to the expected similarity in the SEDs of galaxies at these wavelengths (see previous sections). Indeed, the overlapping J-band data beyond a redshift of two are in good agreement with this color-shifted band.

Figure 1 shows the redshift evolution of the LD for the various wavebands based on the survey data published in the literature for the wavelength bands that we use to extend the previous work of SMS.[5] The upper and lower limits of the bands correspond to the highest and lowest IBL consistent with 68% confidence errors. The error bars on the J- and K-band data taken from Pozzetti et al. (2003) are small in comparison to other data used. Their uncertainty was estimated strictly by considering the range of acceptable Schechter parameters when fitting their LFs. As other authors considered systematic errors such as cosmic variance and extrapolation to the faint end, we have chosen to assign a linear error of 20% to these data to bring their errors more in line with what is typically quoted so that these data do not inordinately influence the fitting routine. The upper and lower limits of the bands correspond to the highest and lowest IBL consistent with 68% confidence errors.

Our method of dealing with the confidence band for redshifts beyond where there are any data for J and K is not critical for the opacity calculation. There is very little contribution to the γ-ray opacities from photons in these wavebands beyond a redshift of 2 because of the short time interval of the emission from galaxies at higher redshifts (see Equation (2)). To verify this, we set an upper limit by assuming that the value of the photon density at $z = 2$ remains constant out to higher redshifts. Since we expect that the LD will drop off at the higher redshifts, this assumption gives an upper limit. We found no appreciable differences in the calculated opacities under this assumption (see next section) as expected.

Having determined the colors between the J, K, L, and M bands, we use them to transform the J and K LDs into the L and M bands and again apply our fitting technique to produce confidence limits for those wavelengths. The color-transformed data along with the confidence bands for L and M can also be seen in Figure 1. We note that the wider resulting confidence bands for L and M occur because we have propagated the error determined from the colors to the J and K data (reflected in the size of the error bars) before running the Monte Carlo simulations and fits. This is as expected, since the band of acceptable photon densities derived from the data should reflect both errors. As in SMS, we then interpolate between the upper limit and lower limit of the confidence bands between the various wavebands separately to find the upper and lower limit rest-frame luminosity densities.

[5] References for the values of $\mathcal{E}_\nu(z)$ used to construct Figure 1 are listed in the legend.

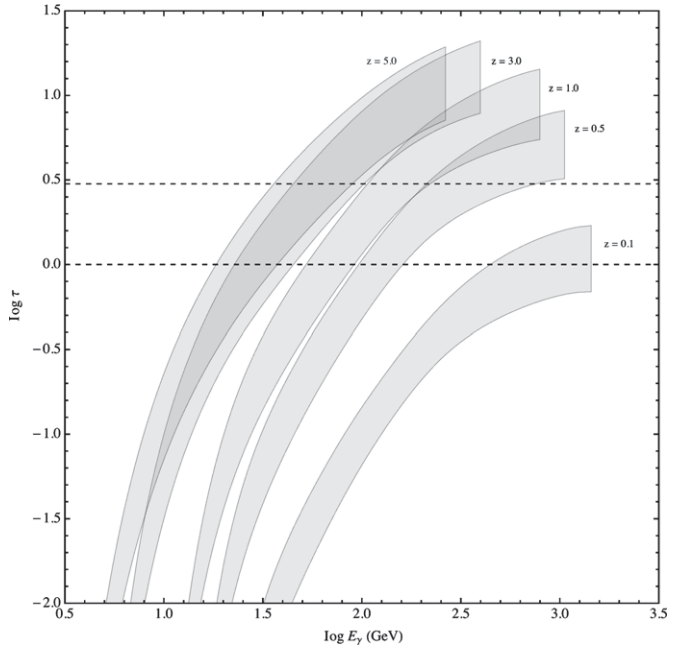

Figure 2. Empirically determined opacities for redshifts of 0.1, 0.5, 1, 3, and 5 extended from SMS. The dashed lines indicate the opacities $\tau = 1$ and $\tau = 3$.

3. DETERMINATION OF THE OPTICAL DEPTH TO γ-RAYS AND RESULTING γ-RAY HORIZON

Using the results of the previous section, the specific emissivity can then be derived for the highest and lowest IBL LDs. The co-moving radiation energy density is then determined from Equation (1). The photon densities derived thereby are given by

$$n(\epsilon, z) = u(\epsilon, z)/\epsilon \tag{4}$$

with $\epsilon = h\nu$, and with $u(\epsilon, z)$ given by Equation (1).

With the co-moving photon density $n(\epsilon, z)$ evaluated, the optical depth for γ-rays owing to electron–positron pair-production interactions with photons of the stellar radiation background can be determined from the expression (Stecker et al. 1992)

$$\tau(E_0, z_e) = c \int_0^{z_e} dz \frac{dt}{dz} \int_0^2 dx \frac{x}{2} \times \int_{\epsilon_{th}}^{\infty} d\epsilon\, (1+z)^3 n(\epsilon, z) \sigma_{\gamma\gamma}[s(z)]. \tag{5}$$

In Equation (5), dt/dz is given by Equation (2), E_0 is the observed γ-ray energy at redshift zero, ϵ is evaluated at redshift z, z_e is the redshift of the γ-ray source, $x = (1 - \cos\theta)$, θ being the angle between the γ-ray and the soft background photon, and the pair-production cross section $\sigma_{\gamma\gamma}$ is zero for the rest system center-of-mass energy $\sqrt{s} < 2m_e c^2$, m_e being the electron mass. Above this threshold, the pair-production cross section is given by

$$\sigma_{\gamma\gamma}(s) = \frac{3}{16}\sigma_T(1-\beta^2)\left[2\beta(\beta^2-2) + (3-\beta^4)\ln\left(\frac{1+\beta}{1-\beta}\right)\right], \tag{6}$$

where σ_T is the Thompson scattering cross section and $\beta = (1 - 4m_e^2c^4/s)^{1/2}$ (Breit & Wheeler 1934; Jauch & Rohrlich 1955).

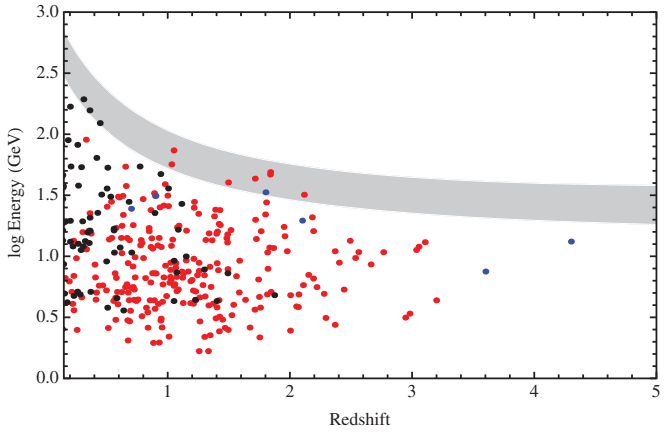

Figure 3. A $\tau = 1$ energy–redshift plot (Fazio & Stecker 1970) showing our uncertainty band results compared with the *Fermi* plot of their highest energy photons from FSRQs (red), BL Lacs (black), and γ-ray bursts (blue) vs. redshift (from Abdo et al. 2010).

(A color version of this figure is available in the online journal.)

As derived in SMS, the pair-production cross section energy has a threshold at $\lambda = 4.8\ \mu\text{m} \cdot E_\gamma(\text{TeV})$, determined from the energy required to produce twice the electron rest mass in the center of mass frame. Since the maximum λ is in the rest-frame M band at 4.8 μm at redshift z, the resulting energy at threshold is $\sim$1.6 TeV at $z = 0$. The energy at interaction in the rest frame is given by $(1+z)E_\gamma$ meaning the maximum γ-ray energy affected by the photon range that we consider is $\sim 1.6\,(1+z)^{-1}$ TeV.

The 68% opacity ranges for $z = 0.1, 0.5, 1, 3$ and 5, calculated using the SMS methods as described above, are plotted in Figure 2. The increasing uncertainties in the γ-ray opacity toward higher redshifts are a reflection of the increasing widths of the uncertainty bands in the luminosity densities shown in Figure 1, as follows from Equations (4) and (5).

Figure 3 shows an energy–redshift plot of the highest energy photons from extragalactic sources at various redshifts from *Fermi* as given by Abdo et al. (2010) along with our 68% confidence band for $\tau = 1$, extending our result from SMS down to a redshift of $z = 0.2$. We stress that our 68% confidence band as shown in Figure 3 is the range of optical depths allowed as derived from our observationally determined IBL results.

4. APPLICATION OF OUR RESULTS TO PKS 1424+240

To show the utility of our results, we consider redshift limits obtained from γ-ray observations of the distant blazar PKS 1424+240. BL Lac objects such as this one typically display bright and featureless continuous spectra making definite spectroscopic determinations of their redshifts challenging. A recent determination of a *lower limit* of the redshift of PKS 1424+240 has been obtained by Furniss et al. (2013). They find $z \geqslant 0.6035$, inferred from *Hubble* observations of the measured positions of Lyman lines from intervening Lyα absorbers at lower redshifts. PKS 1424+240 has been observed at γ-ray energies lower than 100 GeV by *Fermi*-LAT and at energies above 500 GeV by *VERITAS* (Acciari et al. 2010).

Using our opacity results, we can place an *upper limit* on the redshift of this source. A power-law spectrum with index $\sim$1.8 has been determined from *Fermi* for energies below 100 GeV (Furniss et al. 2013). In this energy range, there should be little γ-ray attenuation. Therefore, extending this power-law spectrum out to energies measured by *VERITAS* should represent

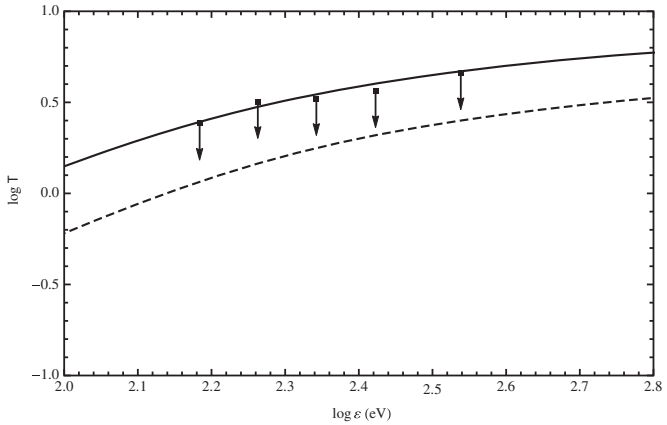

Figure 4. Determination of the upper limit redshift for PKS 1424+240. The points represent the upper limits to the γ-ray opacity derived from the *VERITAS* data. The dashed curve corresponds to our lower limit opacity for $z = .6035$ while the solid curve is our best-fit lower limit opacity to the opacity limits derived from the results shown in Figure 3, corresponding to an upper limit redshift of $z = 1.0$.

an upper limit on its intrinsic spectrum. An upper limit for the opacity for each of the measured γ-ray energies can then be determined from the flux difference between the extended power-law spectrum and the measured fluxes. This upper limit can then be compared with our redshift-dependent opacity curves generated from our lower limit IBL, thereby determining an upper limit on the redshift of PKS 1424+240. Our upper limit on z is found to be 1.0; our lower limit opacities for redshifts greater than $z = 1.0$ exceed the upper limits on the opacity determined from the flux differences. Figure 4 shows the upper limits on the opacities determined from the *VERITAS* data along with our lower limit $z = 1.0$ opacity curve. Aleksić et al. (2014) have used *MAGIC* data to place an upper limit on the redshift of PKS 1424+240 of 0.81. However, the limit obtained by the *MAGIC* collaboration depends on assuming absolute accuracy of the IBL model of Franceschini et al. (2008). The loosening of this limit to a slightly larger upper limit of $z = 1.0$ is a result of using our observationally derived uncertainty band rather than a theoretical model.

5. COMPARISON WITH OTHER RESULTS

Helgason & Kashlinsky (2012, HK) have used a method similar to ours, using galaxy LFs to determine the γ-ray opacity of the universe with uncertainties over the same energy range as considered here. Their results are also model independent. However, their treatment differs from our ours in two respects: (1) the HK uncertainty band is determined by fitting to Schechter function parameterizations with upper and lower limits determined by fitting to faint end slopes of the Schechter functions; we use observationally determined LDs with observational errors combined with our Monte Carlo treatment as described in Section 2.3. Our use of observationally determined errors takes account of systematic effects such as cosmic variance. (2) We use color data as described in Section 2.3 to extrapolate our LDs to higher redshifts, allowing us to make use of more observational data, particularly in the *L* and *M* bands; HK postulate an exponential cutoff in their LDs at higher redshifts. The result of these differences is that our opacities are somewhat larger than those of HK.

Our uncertainty band for the IBL at $z = 0$ (the EBL) is in full agreement with that obtained by Abramowski et al. (2013) using γ-ray spectra from H.E.S.S. (see their Figure 5). Our results are consistent with the work of the *Fermi* collaboration (2010) as shown in our Figure 3. Our results for $z = 1$ are in fair agreement with those of the analyses of the *Fermi* collaboration (Ackermann et al. 2012). Our $\tau = 1$ (horizon) band is consistent with the result of Domínguez et al. (2013).

6. CONCLUSIONS

We have presented an extension of our previous determination of 68% confidence bands giving upper and lower limits on the IBL out to 4.8 μm. This model-independent determination is entirely based on observationally derived LFs from local and deep galaxy survey data and color data. This has enabled us to directly derive both the γ-ray opacity and its observational uncertainties as a function of both energy and redshift out to an energy of $1.6/(1+z)$ TeV for $z \leqslant 5$. We have applied our lower limit opacities to the results of both ground-based air Cerenkov telescope and *Fermi*-LAT observations of PKS 1424+240, allowing us to place a new upper limit on the redshift of this source, viz., $z \leqslant 1.0$, independent of IBL modeling.

We find no direct evidence in our spectral analysis for a required modification of our predicted γ-ray opacities as shown in Figure 4, and for the opacity in the direction of PKS 1424+240, either owing to axion–photon mixing as suggested Meyer & Horns (2013) or by the existence of secondary production effects as suggested by Essey & Kusenko (2013). However, such effects may need to be invoked should a subsequently determined redshift of PKS 1424+240 turn out to be greater than 1.

We thank Amy Furniss for supplying us with the *VERITAS* γ-ray data on PKS 1424+240 that we used in our analysis. We also thank Mariska Kriek for supplying us with galaxy template SEDs.

REFERENCES

Abdo, A., Ackermann, M., Ajello, M., et al. 2010, ApJ, 723, 1082
Abramowski, A., Acero, F., Aharonian, F., et al. 2013, A&A, 550, A4
Acciari, V. A., Aliu, E., Arlen, T., et al. 2010, ApJL, 708, L100
Ackermann, M., Ajello, M., Allafort, A., et al. 2012, Sci, 338, 1190
Aleksić, S., Ansoldi, L., Antonelli, A., et al. 2014, arXiv:1401.0464
Arnouts, S., Walcher, C. J., Le Fèvre, O., et al. 2007, A&A, 476, 137
Bell, E. F., McIntosh, D. H., Katz, N., & Weinberg, M. D. 2003, ApJ, 585, 117
Breit, G., & Wheeler, J. A. 1934, PhRv, 46, 1087
Cirasuolo, M., McLure, R. J., Dunlop, J. S., et al. 2010, MNRAS, 401, 1166
Dai, X., Assef, R. J., Kochanek, C. S., et al. 2009, ApJ, 697, 506
De Angelis, A., Roncadelli, M., & Mansutti, O. 2007, PhRvD, 76, 121301
Domínguez, A., Finke, J. D., Prada, F., et al. 2013, ApJ, 770, 77
Domínguez, A., Primack, J. R., Rosario, D. J., et al. 2011, MNRAS, 410, 2556
Dwek, E., & Krennrich, F. 2013, APh, 43, 112
Essey, W., Kalashev, O. E., Kusenko, A., & Beacom, J. F. 2010, PhRvL, 104, 141102
Essey, W., & Kusenko, A. 2012, ApJL, 751, L11
Essey, W., & Kusenko, A. 2013, arXiv:1310.3440
Fazio, G. G., & Stecker, F. W. 1970, Natur, 226, 135
Feulner, G., Bender, R., Drory, N., et al. 2003, MNRAS, 342, 605
Finke, J. D., Razzaque, S., & Dermer, C. D. 2010, ApJ, 712, 238
Franceschini, A., Rodighiero, G., & Vaccari, M. 2008, A&A, 487, 837
Furniss, A., Williams, D. A., Danforth, C., et al. 2013, ApJL, 768, L31
Gilmore, R. C., Madau, P., Primack, J. R., et al. 2009, MNRAS, 399, 1694
Heath-Jones, D., Peterson, B. A., Colless, M., & Saunders, W. 2006, MNRAS, 369, 25
Hill, D. T., Driver, S. P., Cameron, E., et al. 2010, MNRAS, 404, 1215
Helgason, K., & Kashlinsky, A. 2012, ApJL, 758, L13
Jauch, J. M., & Rohrlich, F. 1955, The Theory of Photons and Electrons (Cambridge, MA: Addison-Wesley)
Kneiske, T. M., & Dole, H. 2010, A&A, 515, A19

Kneiske, T. M., Mannheim, K., & Hartmann, D. H. 2002, A&A, 386, 1
Kochanek, C. S., Pahre, M. A., & Falco, E. E. 2001, ApJ, 560, 566
Kriek, M, Labbé, I., Convoy, C., et al. 2010, ApJL, 722, 64
Kriek, M., van Dokkum, P. G., Whitaker, K. E., et al. 2011, ApJ, 743, 168
Ly, C., Malkan, M. A., Hayashi, M., et al. 2011, ApJL, 735, L91
Malkan, M. A., & Stecker, F. W. 1998, ApJ, 496, 13
Malkan, M. A., & Stecker, F. W. 2001, ApJ, 555, 641
Meyer, M., & Horns, D. 2013, arXiv:1310.2058
Pozzetti, L., Cimatti, A., Zamorani, G., et al. 2003, A&A, 402, 837
Salamon, M. H., & Stecker, F. W. 1998, ApJ, 493, 547
Somerville, R. S., Gilmore, R. C., Primack, J. R., & Domínguez, A. 2012, MNRAS, 423, 1992
Stecker, F. W., De Jager, O. C., & Salamon, M. H. 1992, ApJL, 390, L49
Stecker, F. W., Malkan, M. A., & Scully, S. T. 2006, ApJ, 648, 774
Stecker, F. W., Malkan, M. A., & Scully, S. T. 2012, ApJ, 761, 128
Stefanon, M., & Marchesini, D. 2013, MNRAS, 429, 881